Modelling and remote sensing of water temperature of the Yenisei river (Russia)

Modelling and remote sensing of water temperature of the Yenisei river (Russia)

N Y Shaparev[1,2], **Y I Shokin**[3], **and O E Yakubailik**[1,2]

[1] Institute of Computational Modelling of the Siberian Branch of the Russian Academy of Sciences, Russia, 660036, Krasnoyarsk, Akademgorodok 50/44.
[2] Siberian Federal University, Russia, 660041, Krasnoyarsk, Svobodny pr., 79.
[3] Institute of Computational Technologies of the Siberian Branch of the Russian Academy of Sciences, 630090, Russia, Novosibirsk, Academician M.A. Lavrentiev avenue, 6.

This study was performed with financial support of the RFBR and the Government of the Krasnoyarsk Territory, research project no. 18-41-242006p_mk

Abstract. The summertime hydrothermal regime of the Yenisei River downstream of the Krasnoyarsk hydroelectric power plant is modeled using a remote sensing and deterministic approach. The Fourier equation is used, and the following physical processes contributing to the heat exchange between the water and the surroundings are taken into consideration: the absorption of direct and scattered solar radiation by water, the absorption of downwelling thermal infrared radiation (TIR) from the atmosphere by water surface, TIR back from the water surface, the convection of heat and the heat loss due to evaporation of water. A clear-skies river thermal regime under no wind condition is studied at 32-km downstream the power plant, and the obtained results are compared against remote sensing data.

1. Introduction

The Yenisei River in terms of runoff is the largest in Russia (599 km^3/year) and the seventh largest in the world (1.5% of the global runoff) [1]. The stream flows in the meridian direction through various climatic zones. The river basin with a total area of 2.6×10^6 km^2 houses the largest region in Russia, Krasnoyarsky Krai. There are 6 hydroelectric power plants (HPP) in the basin of the river. One of them, the Krasnoyarsk HPP, is among the top ten world's most powerful hydroelectric power plants (6000 MW) and the key anthropogenic factor influencing the Yenisei river. The river dam is 124 m in height and 1065 m in width. Upstream, above the dam, a reservoir of 73 km^3 capacity has been built. Depending on the climatic and economic conditions, the water discharge ranges from 7000 m^3sec^{-1} to 2000 m^3sec^{-1}. Water from the bottom strata of this reservoir flows through the dam and enters the afterbay of the Krasnoyarsk HPP. The incoming water temperature varies over the year from 2ºC to 12ºC. As a result, downstream of the HPP the summer water temperatures are lower and the winter temperatures are higher than those before the stream was regulated. Temperature is an important parameter, since it influences the behavior of the hydrophysical, hydrochemical, and hydrobiological processes.

The water temperature, in turn, depends on the meteorological conditions [2, 3], including solar radiation, air temperature, relative humidity, wind speed, cloud cover, and barometric pressure. The stream water temperature is also affected by the discharge of water, the inflow temperature, and the morphometric river characteristics [4–12].

The heat exchange mechanism underlies the following physical processes in a river: absorption of solar radiation by water, TIR emission and TIR absorption from the atmosphere by water, convection and evaporation, heat transport due to the river flow and thermal conductivity, as well as the heat exchange between the water and streambed.

Temperature is a key indicator of the natural environment. It can be measured by ground based methods or satellite data. Remote sensing techniques provide temperature data on a regular grid with high spatial resolution, with incomparably greater detail than the data of several irregular weather or hydrological stations of official governmental services [13].

The first images of the Earth from space in the thermal infrared range were obtained by American meteorological satellites in the 1960s. Despite the fact that these satellite data had low spatial resolution and practical application, they showed the principal possibility of solving a number of problems in the field of environmental studies by remote sensing. Currently one of the most interesting satellites which regularly surveys the earth's surface in the thermal infrared (IR) range is Landsat 8. The recorded IR data has a high spatial resolution of 100 meters per pixel, and the repeatability of the survey is 16 days. Landsat 8 is not the only thermal infrared satellite, but because of a combination of data availability and high spatial resolution, it is considered to be the leader in the subject area [14].

2. Subject of research

Here we consider the summertime hydrothermal regime in a 32-km river reach downstream of the Krasnoyarsk HPP on July 3, 2016 based on a deterministic modeling approach. We apply a physically-based heat balance modeling approach, since it requires minimum additional information, which is of particular importance for the poorly developed areas of the Yenisei River. The physical heat exchange processes include absorption of direct and scattered solar radiation by water, absorption of downwelling thermal infrared radiation (TIR) from the atmosphere by the water surface, TIR back from the water surface, convection of heat and heat loss due to evaporation of water. To carry out mathematical simulation, we use the Fourier equation. We show that under our conditions the water flow is turbulent and the thermal conductivity of water can be safely ignored. Next we switch to a coordinate system moving with water and end up with a simple differential equation for water temperature. With this equation we can predict the longitudinal water temperature fluctuation along the river at various times considering real morphometric characteristics.

The method of assessing the temperature of the Earth's land surface and, in particular, the water surface, is the subject of numerous studies [15, 16]. Unlike a number of other satellite data, Landsat temperature data must be calculated. Each pixel of Landsat 8 TIR data is stored as Digital Numbers (DNs) with a value between 0 and 2^{15}. To obtain the actual surface temperature, we need first to a) convert these DNs to top-of-the-atmosphere (ToA) radiance values, and then b) convert the ToA radiance values to ToA brightness temperature in Kelvin. The last step is the estimation of Land (Water or Sea) Surface Temperature (LST). Land Surface Temperature can be calculated from ToA Brightness Temperature T_B [17]:

$$T = T_B/[1 + (\lambda \cdot T_B/c_2) \cdot ln(\varepsilon_w)],$$

where λ = wavelength of emitted radiance, $c_2 = h \cdot c/s = 1.4388 \cdot 10^{-2}$ m K,
h = Planck's constant = $6.626 \cdot 10^{-34}$ J s, c = velocity of light = $2.998 \cdot 10^{8}$ m/s,
s = Boltzmann constant = $1.38 \cdot 10^{-23}$ J/K, ε_w = emissivity of the water surface.

3. Mathematical Modeling of the hydrothermal regime

Water from the upstream reservoir is released through the dam and enters the afterbay of surface width B (m) and cross-sectional area S (m^2). The water discharge through the dam body is characterized by the quantity Q ($m^3 sec^{-1}$). The mean streamflow velocity V (km hr^{-1}) is

$$V = \frac{Q}{S}. \tag{1}$$

The hydrothermal river regime in this situation can be described by the Fourier equation [18]:

$$\frac{\partial T_w(x,t)}{\partial t} = -V(x)\frac{\partial T_w(x,t)}{\partial x} + D\frac{\partial^2 T_w(x,t)}{\partial x^2} + \frac{W(t)}{\rho c}\frac{B(x)}{S(x)}. \tag{2}$$

The first term in the right-hand side refers to the rate of change in the temperature caused by advection, the second one is associated with the rate of change in the temperature due to dispersion, and the third term describes the heat exchange between the water and the surrounding environment. Here T_w (ºC) is the cross-sectional average water temperature in degrees Celsius, t (hour) is time, x (km) is the distance downstream of the dam, ρ (10^3 kg m^3) is the specific water density, c ($4.19 \cdot 10^{-3}$ J kg^{-1} ºC^{-1}) is the specific heat of water, D ($m^2 sec^{-1}$) is the dispersion coefficient in the direction of the flow, W ($W \cdot m^{-2}$) is the heat transfer power between the water and the surroundings, which equals

$$W(t) = W_s + W_{ss} + W_a - W_w + W_c - W_e, \tag{3}$$

where W_s and W_{ss} are, respectively, the direct and scattered downwelling solar radiation absorbed by water; W_a is the atmospheric TIR absorbed by water; W_w is the TIR from the water surface to the atmosphere; W_c is the convective heat transfer from the atmosphere to the water, and W_e is the loss of heat due to evaporation. In this paper we deal with uniform streams for which Q is independent of time. In this situation the streambed temperature adjusts to the temperature of water and, therefore, the thermal exchange between the water and the streambed surface can be neglected [18].

For $V \gg 10^{-3}$ m sec^{-1} the thermal conductivity can be neglected. Then in the system of coordinates moving at a velocity $V(x)$ equation (2) is rewritten as

$$\frac{dT_w(t)}{dt} = \frac{W(t)}{\rho c}\frac{B\left(x(t)\right)}{S\left(x(t)\right)}, \tag{4}$$

whose solution is found from the expression

$$T_w(t) = \frac{1}{\rho c}\int_{t_0}^{t}\frac{B(x(t))}{S(x(t))}W(t)dt + T_w(0,t_0), \quad x(t) = Q\int_{t_0}^{t}\frac{dt}{S(x(t))}. \tag{5}$$

Here $T_w(0,t_0)$ is the outflow temperature of water leaving the dam at time t_0.

The power of extraterrestrial solar radiation equals [19, 20]

$$F = F_0 E\cos\theta, \quad \cos\theta = \sin\varphi\cdot\sin\delta + \cos\varphi\cdot\cos\delta\cdot\cos\omega t', \tag{6}$$

where $F_0 = 1367\ \mathrm{Wm}^{-2}$ is the solar constant, E is the eccentricity correction factor, θ is the zenith angle, t' is the time from noon, and ω is the rotational speed of the Earth around its polar axis. Here $\varphi = 55.94^{\circ}$ is the geographic latitude of the HPP location. The solar declination on July 3, 2016 was $\delta = 22.97^{\circ}$ and $E = 0.966$. Note that the diurnal variation of δ was insignificant and, therefore, the sunrise and sunset times are both determined by the condition $F = 0$. From (6) we have

$$\cos\omega t_0 = -\mathrm{tg}\varphi\cdot\mathrm{tg}\delta. \tag{7}$$

Consequently, the negative root of the expression, $-\omega t_0$, refers to the sunrise and the positive one, ωt_0, to the sunset. Since t' is the time from noon, we further have

$$\cos \omega t' = \cos\left(\pi \frac{t - t_n}{12} \right), \tag{8}$$

where t_n is the time of solar noon and t is the time from midnight. From (7) we have t_{sr} = 4.06 hours for the sunrise and t_{ss} = 21.57 hours for the sunset. Then the length of day is 15.51 hours and the time of noon will be t_n =12.81 hours. The temporal behaviour of the power of extraterrestrial solar radiation is described by expression (6) and is shown in Figure 1 (curve 1).

When solar radiation enters the Earth's atmosphere, a part of the incident energy is removed by scattering and a part by absorption and, according to the Bouguer-Lambert-Beer law, the power of solar radiation reaching the ground (water) surface is

$$F' = F \cdot \exp\left(-\frac{\tau_0}{\cos\theta} \right), \tag{9}$$

where the clear sky optical thickness of the atmosphere is $\tau_0 \simeq 0.12$ taking into account the scattered radiation [19, 20].

The power of direct and scattered solar radiation incident on the water surface is found from expression (9) and is shown in Figure 1 (curve 2).

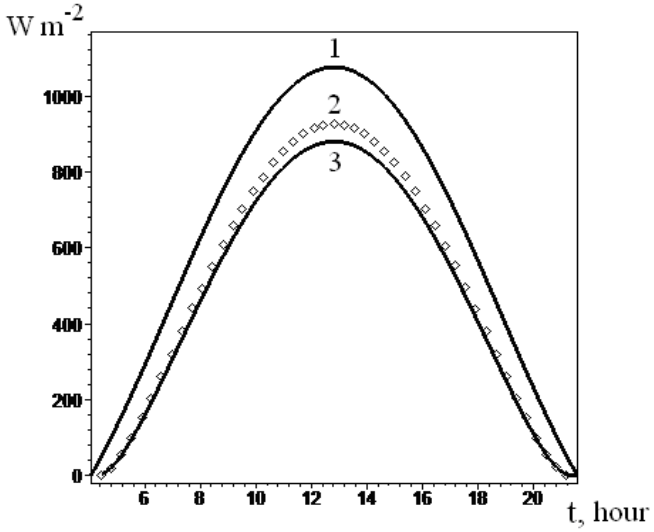

Figure 1. Temporal dependence of solar radiation power: 1 – incident on the Earth's atmosphere, 2 – transferred through the atmosphere, 3 – absorbed by water.

Upon reaching a plane water surface, solar radiation is partially reflected. The reflection coefficient *R* is calculated by the Fresnel's formula. The remaining part of solar energy (1-R) is absorbed by water. Thus,

$$W_s + W_{ss} = (1 - R)F'. \tag{10}$$

The power of solar radiation absorbed by water is shown in Figure 1 (curve 3).

The water surface emits TIR defined by the Stefan-Boltzmann law as

$$W_w = \varepsilon_w \sigma (273 + T_w)^4, \tag{11}$$

where ε_w is the emissivity of the water surface, which is $\varepsilon_w = 0.995$ according to [21]. For $T_w = 7.2°C$ we have $W_w = 290\,\mathrm{W\,m^{-2}}$. While emitting this energy the water gets colder.

Atmospheric radiation is also determined by the Stefan-Boltzmann law. Over years, various empirical formulas have been proposed to calculate the atmospheric emission coefficient ε_a. An overview of these is given in [22]. Our analysis has shown that the best formula for our situation is the one proposed in [23], because the optical thickness of the atmosphere in the wavelength range of 9.8 μm where the atmosphere emits is close to unity [24]:

$$\varepsilon_a = 1 - 0.4 \cdot \exp\left(-\frac{100 e_a}{T_a + 273}\right), \tag{12}$$

where T_a is the temperature of the atmosphere in ºC, and e_a (mb) is the atmospheric water vapor pressure.

Now we can carry out calculations for July 3, 2016. At noon T_a = 26 ºC and the humidity was H = 45%, at midnight T_a = 14 ºC, H = 85%. Then we have $\varepsilon_a = 0.99$, $W_a = 460\,\mathrm{W\,m^{-2}}$ at noon and $\varepsilon_a = 0.99$, $W_a = 390\,\mathrm{Wm^{-2}}$ at midnight. The atmospheric thermal infrared radiation is absorbed by water surface and increases the water temperature.

The energy spent on water evaporation, W_e, is estimated as [25–27]

$$W_e = \rho L\, f(w)(e_s - e_a), \tag{13}$$

where $L = 2.26 \cdot 10^6$ J kg^{-1} is the latent heat of evaporation, e_s is the saturation vapor pressure. When the wind velocity is $w = 0$, we have $f \simeq 3 \cdot 10^{-9}\,(\mathrm{mb^{-1} m s^{-1}})$ according to the data from [28]. For the quoted data we have $W_e = 31\,\mathrm{W\,m^{-2}}$ at noon and W_e = 4.6 W m^{-2} at midnight, which results in a drop of the water temperature.

The convective heat flux is estimated as [29]:

$$W_c = 0.61 \rho L\, f(T_w - T_a). \tag{14}$$

Thus, the convective heating is 25 W m^{-2} at noon and 1.3 W m^{-2} at midnight. The difference between the evaporation and convection is 6 W m^{-2} during the daytime and 3.3 W m^{-2} at night. Hence, the heat budget is dominated by evaporation and the water gets colder.

We consider a 32-km reach of the Yenisei River downstream the dam of the Krasnoyarsk HPP. The reach is divided by 5 cross-section lines (7 km, 17 km, 22 km, 28 km, and 32 km). The streamflow velocity is assumed constant from section to section and is found from equation (1) at Q = 2900 m^{3}sec^{-1}; S is equal to the cross-sectional area of the downstream lowest reach section. The flow time between the section lines is found as the section-to-section distance divided by the flow velocity. The water temperature $T_W(0, t_0)$ = 7.2 ºC remained constant during the time period under consideration. The power emitted by water is 290 Wm^{-2}. The atmospheric radiation power was assumed to be 460 Wm^{-2} in the daytime and 390 Wm^{-2} at night. The difference in power between the evaporation and convection is 6 Wm^{-2} during the daytime and 3.3 Wm^{-2} during the nighttime.

The data for each cross-section of the river from high resolution remote sensing imagery and river navigation (pilot) maps with data on the depth of the river were calculated. The results are shown in Table 1. It also shows the streamflow velocity and the time of the flow between the adjacent sections Δt_i, as well as the B/S relation.

Table 1. Morphometric and hydrophysical characteristics of studied part of the river.

River cross-section number Distance from dam	1 (7 km)	2 (17 km)	3 (22 km)	4 (28 km)	5 (32 km)
Width *B*, m	640	652	544	767	830
Cross-sectional area *S*, m^2	1883	1738	1968	1667	2260
Streamflow velocity, km/hour	5.4	6.0	5.3	6.3	4.6
Flow time between adjacent cross-section lines, Δt_i, hours	0.90	1.67	0.94	0.96	0.87
Relation *B*/*S*, m^{-1}	0.34	0.37	0.28	0.46	0.37

The change in the water temperature in each section of the river, Δt_i **,** will be determined according to formula (5) by the expression

$$\Delta T_i = \frac{1}{\rho c}\frac{B_i(x_i(t))}{S_i(x_i(t))}\left[A(t_i) - A(t_{i-1})\right] + \left[W_a - W_w - W_e + W_c\right]\Delta t_i\,, \qquad (15)$$

where $A(t_{i-1})$ (Wm^{-2}hour) is the solar energy absorbed by water at the river part number *i* from the sunrise to the time t_{i-1}, $A(t_i)$ is the solar energy absorbed by the water from the sunrise to time t_i. Respectively, their difference in formula (15) is equal to the solar energy absorbed by the water in the part of the river between *i-1* and *i* cross-section lines.

In order to compare the temperature change along the river based on the solar energy absorption with the values obtained from remote sensing data, it is necessary to perform calculations of the solar energy absorption corresponding to the date and time of the satellite imagery. In our case the Landsat-8 satellite took a survey of the study area on July 3, 2016 at about 11:50 local time (in the decimal format it is 11.83).

The study area is divided into 5 segments, and each of them has all necessary parameters. Knowing the water flow rates on all segments, it is possible to determine the timing of the displacement of the water in the river. In particular, the water droplets located at the time of shooting in cross-section 1 passed through the dam at 10.93. The water droplets located at the time of shooting in cross-section 2 passed through cross-section 1 at 10.16, and through the dam at 9.26. All these data for all cross-sections are grouped in Table 2.

Table 2. Timing of displacement of the water in the river.

River cross-section number Distance from dam	at dam (0 km)	1 (7 km)	2 (17 km)	3 (22 km)	4 (28 km)	5 (32 km)
Timing for water part 1, hour	10.93	11.83				
2	9.26	10.16	11.83			
3	8.32	9.22	10.89	11.83		
4	7.36	8.26	9.93	10.87	11.83	
5	6.49	7.39	9.06	10.00	10.96	11.83

For all moments of time in Table 2, the corresponding values of absorbed solar energy were calculated based on the above formula (10). The results are presented in Table 3.

Table 3. The amount of solar energy absorbed by water from sunrise to a given point in time.

Time, hour	6.49	7.36	7.39	8.26	8.32	9.06	9.22	9.26
A, Wm^{-2}hour	196	465	478	854	884	1298	1403	1418
Time, hour	9.93	10.00	10.16	10.87	10.89	10.93	10.96	11.83
A, Wm^{-2}hour	1875	1955	2043	2592	2615	2645	2664	3401

Then calculations of the water temperature changes for different cross-sections using the expression (15) were performed. For example, for a portion of water that reached cross-section 2 at the time of the survey, the 1st section (from the dam to section 1) passed from time 9.26 to 10.16, the water temperature increased by 0.22 °C, and the second section (from section 1 to section 2) passed from time 10.16 to 11.83, and the temperature increase was 0.52 °C. Thus, the total temperature increase of the considered part of water was 0.74 °C. All these results of calculations are collected in Table 4. Figure 2 summarizes the obtained results on the temperature change along the river (curve 1).

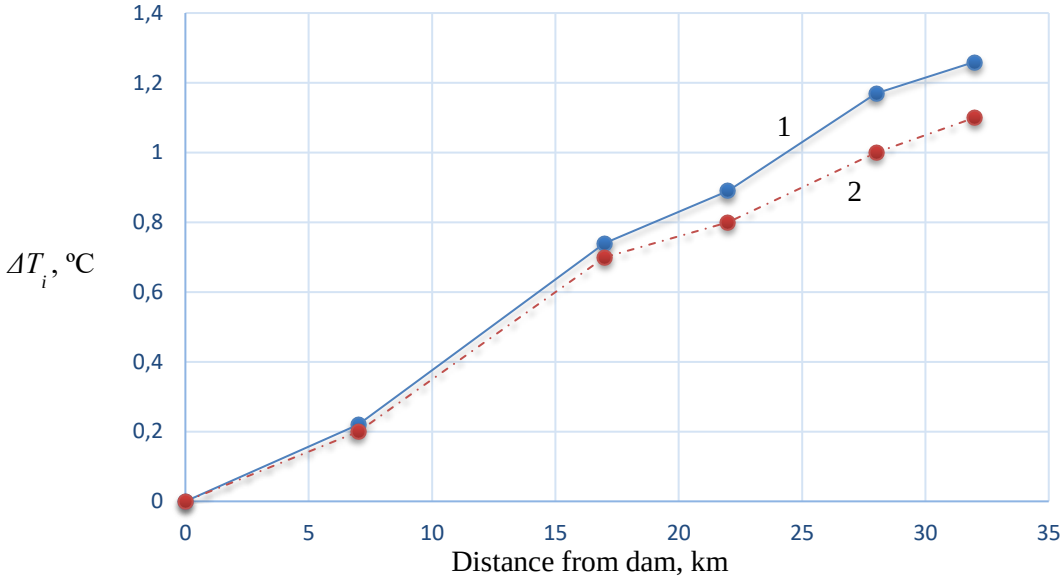

Figure 2. Water temperature depending on distance: mathematical modeling (1) and remote sensing data (2).

Table 4. Water temperature increasing by absorbing solar energy.

River part	dam – 1	1 – 2	2 – 3	3 – 4	4 – 5	Total ΔT, ºC
ΔT for water part 1, ºC	0.26					0.26
2	0.22	0.52				0.74
3	0.19	0.47	0.23			0.89
4	0.15	0.42	0.21	0.38		1.16
5	0.12	0.34	0.19	0.34	0.27	1.26

4. Remote sensing temperature data preparation

The relevant tarball file containing the data was downloaded using the United States' Geological Survey's (USGS) EarthExplorer tool; the area of interest was encompassed by [scene identifier: path 143 row 021] in the WRS-2 scheme, scene id = LC81430212016185LGN00. When the tarball is unpacked fully, the band used from the TIRS instrument is band 10; the relevant .TIF file is ["identifier"_B10.tif], and it was clipped to the study area.

In accordance with the standard procedure noted above, the calculations were carried out. At the first step Dark Object Subtraction (DOS) atmospheric correction was performed. Then DNs were converted to top-of-the-atmosphere (ToA) radiance values, the ToA radiance values to ToA brightness temperature, and the ToA brightness temperature to Land (Water) Surface Temperature in Celsius degrees. Open source GIS software QGIS 2.18 with the Semi-Automatic Classification Plugin (SACP) plug-in was used to process the satellite data [30].

On the basis of the prepared satellite temperature map data, estimation of the water temperature at the mentioned cross-section lines was performed. Figure 2 summarizes the obtained results on the temperature change along the river (curve 2). It shows the data of the calculations and the results of remote sensing data processing.

5. Conclusions

We have proposed a simple model for simulating the summertime hydrothermal regime of a river based on the calculation of water temperature in a coordinate system moving with the water. A physically based estimation of the water heat budget takes into account the absorption of solar radiation by water surface, the emission and absorption of atmospheric TIR by water, the convective heating of water, as well as the heat loss due to evaporative processes. The temporal fluctuation pattern of direct and scattered solar radiation depends on the zenith angle and atmospheric absorption. The dominant water heating factor is solar radiation during the daytime and atmospheric TIR at night. The water temperatures at 32 km downstream of the Krasnoyarsk HPP on the Yenisei River computed using the above-proposed model with consideration of morphometric characteristics are close to the temperatures obtained from Landsat 8 satellite remote sensing data. This proves that the physical-mathematical model provides an adequate description of the actual hydrothermal processes.

The above-proposed approach, which combines methods of physical and mathematical modeling and remote sensing, is promising and effective for use in problems and models associated with specific areas and taking into account their specificity in the conditions of natural and climatic changes. It gives high-quality scientific and practical results in management decision-making for various tasks of analysis, assessment, and monitoring of the environment.

Acknowledgments

The authors are grateful to NASA (National Aeronautics and Space Administration) and USGS (United States Geological Survey) for making it possible to use Landsat satellite data.

References

[1] Dingman S 2015 *Physical Hydrology* (Long Grove, Illinois, USA: Waveland Press, Inc.)
[2] Edinger J, Duttweiler D and Geyer J 1968 The response of water temperatures to meteorological conditions *Water Resour. Res.* **4** 1137-43
[3] Edinger J , Brady D and Geyer J 1974 Heat exchange and transport in the environment, *Report No14* (Palo Alto, California, USA: Electric Power Res. Inst. Publ. No EA-74-049-00-3)
[4] Morse W 1972 Stream temperature prediction under reduced flow *J. Hydraul. Div.* **98** 1031-47
[5] Brown G and Krygier J 1970 Effects of clear-cutting on stream temperature *Water Resour. Res.* **6** 1133-39
[6] Brown G 1969 Predicting temperatures of small streams *Water Resour. Res.* **5** 68-75
[7] Grant P 1977 Water temperatures on the Ngaruroro River at three stations *J. Hydrol. (NZ)* **16** 148-57
[8] Hockey J, Owen I and Tepper N 1982 Empirical and theoretical models to isolate the effect of discharge on summer water temperatures in the Hurunui River *J. Hydrol. (NZ)* **21** 1-12
[9] Churchill M 1963 Control of temperature through streamflow regulation *Proc. Symp. on Stream Flow Regulation for Quality Control* (Cincinnati, Ohio, USA) pp 179-192
[10] Mitchell A, James C and Edinger J 1995 Analysis of flow modification on water quality in Nechako River *J. Energy Eng.* **121** 73-80
[11] Gu R, Montgomery S and Austin T 1998 Quantifying the effects of stream discharge on summer river temperature *Hydrol. Sci. J.* **43** 885-904
[12] Tung C, Yang Y, Lee T and Li M 2007 Modification of a stream temperature model with Beer's law and application to Gaoshan Creek in Taiwan *Ecol. Model.* **200** 217-24

[13] Handcock R, Gillespie A, Cherkauer K, Kay J, Burges S and Kampf S 2006 Accuracy and uncertainty of thermal-infrared remote sensing of stream temperatures at multiple spatial scales *Rem. Sens. of Env.* **100** 427-40
[14] Jiménez-Muñoz J, Cristóbal J, Sobrino J, Soria G, Ninyerola M and Pons X 2009 Revision of the single-channel algorithm for land surface temperature retrieval from Landsat thermal-infrared data *IEEE Trans. Geosci. Remote Sens.* **47** 339-49
[15] Coll C, Galve J, Sanchez J and Caselles V 2010 Validation of Landsat-7/ETM+ thermal-band calibration and atmospheric correction with ground-based measurements *IEEE Trans. Geosci. Remote Sens.* **48** 547-55
[16] Qin Z, Karnieli A and Berliner P 2001 A mono-window algorithm for retrieving land surface temperature from Landsat TM data and its application to the Israel-Egypt border region *Int. J. Remote Sens.* **22** 3719-46
[17] Weng Q, Lu D and Schubring J 2004 Estimation of land surface temperature-vegetation abundance relationship for urban heat island studies *Rem. Sens. of Env.* **89** 467-83
[18] Sinokrot B and Stefan H 1993 Stream temperature dynamics: measurements and modelling *Water Resour. Res.* **29** 2299-312
[19] Kondratyev K Ya. 1969 *Radiation in the Atmosphere* (New York: Academic Press)
[20] Iqbal M 1983 *An introduction to solar radiation* (San Jose: Academic Press)
[21] Handcock R, Torgersen C, Cherkauer K, Gillespie A, Tockner K, Faux R and Tan J 2012 Thermal infrared remote sensing of water temperature in riverine landscapes *Fluvial Remote Sensing for Science and Management* ed Charbonneau P and Piegay H. (John Wiley and Sons, Ltd.) chapter 5 pp 85-113
[22] Flerchinger G, Xaio W, Marks D, Sauer T and Yu Q 2009. Comparison of algorithms for incoming atmospheric long-wave radiation. *Water Resour. Res.* **45** W03423
[23] Iziomon M, Mayer H and Matzarakis A 2003 Downward atmospheric longwave irradiance under clear and cloudy skies: Measurement and parametrization *J. Atmosph. Solar Terrestrial Phys.* **65** 1107-16
[24] Rees W 2001 Physical Principles of Remote Sensing (Cambridge: Cambridge University Press)
[25] Shulyakowski L 1969 Formula for computing evaporation with allowance for the temperature of free water surface *Sov. Hydrol. Sel. Papers* **6** 566-73
[26] Ryan P and Harleman D 1973 An analytical and experimental study of transient cooling pond behaviour *Rep. No 161* (Parsons Laboratory for Water Resources and Hydrodynamics, Massachusetts Institute of Technology, Cambridge)
[27] Gulliver J and Stefan H 1986 Wind function for sheltered stream. *J. Environ. Eng.* **112** 1-14
[28] Boyd M and Kasper B 2003 Analytical methods for dynamic open channel heat and mass transfer: methodology for heat source model version 7.0.
Available at: https://www.oregon.gov/deq/FilterDocs/heatsourcemanual.pdf
[29] Bowen I 1926 The ration of heat losses by conduction and by evaporation from any water surface *Phys. Rev.* **27** 749-87
[30] Congedo L 2016 Semi-Automatic Classification Plugin Documentation
DOI: http://dx.doi.org/10.13140/RG.2.2.29474.02242/1